Minimization of Torque Ripple in PWM AC Drives

Kaushik Basu, J. S. Siva Prasad, and G. Narayanan, *Member, IEEE*

***Abstract*—A pulsewidth modulation (PWM) technique is proposed for minimizing the rms torque ripple in inverter-fed induction motor drives subject to a given average switching frequency of the inverter. The proposed PWM technique is a combination of optimal continuous modulation and discontinuous modulation. The proposed technique is evaluated both theoretically as well as experimentally and is compared with well-known PWM techniques. It is shown that the proposed method reduces the rms torque ripple by about 30% at the rated speed of the motor drive, compared to conventional space vector PWM.**

***Index Terms*—Harmonic analysis, harmonic distortion, induction motor drive, pulsewidth modulation (PWM), pulsewidth-modulated inverter, torque pulsation.**

I. Introduction

THE OUTPUT of a pulsewidth-modulated voltage source inverter contains harmonic voltages in addition to the fundamental voltage. When applied on a three-phase induction motor, these harmonic voltages result in harmonic currents and pulsating torques [1]–[4].

Extensive research has been carried out to assess and reduce the line current ripple in pulsewidth modulation (PWM) inverters operating at a given switching frequency [1]–[14]. This paper extends the previous research [3], [10], [11] on evaluating and reducing the torque ripple in inverter-fed drives. Conventional space vector PWM (CSVPWM) with equal division of zero vector time is known to produce less torque ripple than sine-triangle PWM (SPWM) [3]. This paper shows that the optimal continuous PWM (OCPWM) [6], [7] leads to further reduction in torque pulsation. Further, this paper proposes a combination of OCPWM and discontinuous PWM that leads to still lower values of rms torque ripple, particularly at higher speeds of constant V/f induction motor drives. Theoretical and experimental results on a 3-kW induction motor drive are presented.

II. Current Ripple and Torque Ripple

A three-phase voltage source inverter produces eight switching states, comprising two zero states and six active states, as shown in Fig. 1(a). The corresponding voltage vectors are shown normalized with respect to the dc bus voltage $V_{\rm dc}$. In a continuous modulation technique such as SPWM or conventional space vector PWM (CSVPWM), the inverter state applied changes from one zero state (e.g., 0) to the other zero state (e.g., 7) through two active states in any half-carrier cycle or subcycle (T_s). If in the three-phase voltage reference (v_R, v_Y, v_B), $v_R > v_Y > v_B$ [i.e., if the reference vector $V_{\rm ref}$ is in sector I, as shown in Fig. 1(a)], then the switching sequence in the given subcycle is 0127 or 7210, as illustrated in Fig. 1(b). The active states 1 and 2 are applied for durations T_1 and T_2, respectively, as shown in (1), where V_P is the peak of the bipolar triangular carrier. The zero vector is applied for the remaining duration T_z [2], [5]–[8], [10], [15], which is described as follows:

$$\begin{aligned} T_1 &= \frac{V_{\rm ref}\sin\left(\frac{\pi}{3}-\alpha\right)}{\sin\left(\frac{\pi}{3}\right)}T_s = \frac{(v_R - v_Y)}{2V_P}T_s \\ T_2 &= \frac{V_{\rm ref}\sin(\alpha)}{\sin\left(\frac{\pi}{3}\right)}T_s = \frac{(v_Y - v_B)}{2V_P}T_s \\ T_z &= T_s - T_1 - T_2. \end{aligned} \tag{1}$$

In general, the duration T_z is divided between the two zero states 0 and 7, as shown in (2). While x always equals 0.5 with CSVPWM, the ratio of apportioning differs with the three-phase reference (v_R, v_Y, v_B) in the case of SPWM. Different continuous and discontinuous modulation methods primarily differ in terms of this fraction x, which leads to differences in the spectral properties of the waveforms generated [2], [6], [7], i.e.,

$$T_0 = xT_z \quad T_7 = (1-x)T_z, \quad 0 \le x \le 1. \tag{2}$$

There is an instantaneous error between the applied voltage vector (e.g., $\mathbf{V}_1$) and the reference vector $\mathbf{V}_{\rm ref}$, as shown in Fig. 1(c). This error voltage causes the line current ripple [10]. For a given value of x, the locus of the tip of the current ripple vector over a subcycle is given as shown in Fig. 1(c). The components of the current ripple vector along the d- and q-axes are shown in Fig. 1(d). The error volt-second quantities Q_1, Q_2, Q_z, and D in Fig. 1(d) are defined in the following equation, where l is the leakage inductance of the machine:

$$\begin{aligned} Q_1 &= \frac{V_{\rm dc}}{l}\left[\cos(\alpha) - V_{\rm ref}\right]T_1 \\ Q_2 &= \frac{V_{\rm dc}}{l}\left[\cos\left(\frac{\pi}{3}-\alpha\right) - V_{\rm ref}\right]T_2 \\ Q_z &= -\frac{V_{\rm dc}V_{\rm ref}T_z}{l} \\ D &= \frac{V_{\rm dc}\sin(\alpha)T_1}{l}. \end{aligned} \tag{3}$$

Manuscript received April 10, 2008; revised July 28, 2008. First published August 26, 2008; current version published January 30, 2009. This work was supported by the Department of Science and Technology, Government of India, under the Science and Engineering Research Council Fast Track Scheme for Young Scientists.

K. Basu was with the Department of Electrical Engineering, Indian Institute of Science, Bangalore 560012, India. He is now with the Department of Electrical Engineering, University of Minnesota, Minneapolis, MN 55455-0213 USA (e-mail: kaushik.iisc@gmail.com).

J. S. Siva Prasad and G. Narayanan are with the Department of Electrical Engineering, Indian Institute of Science, Bangalore 560012, India (e-mail: prasad@ee.iisc.ernet.in; gnar@ ee.iisc.ernet.in).

Digital Object Identifier 10.1109/TIE.2008.2004391

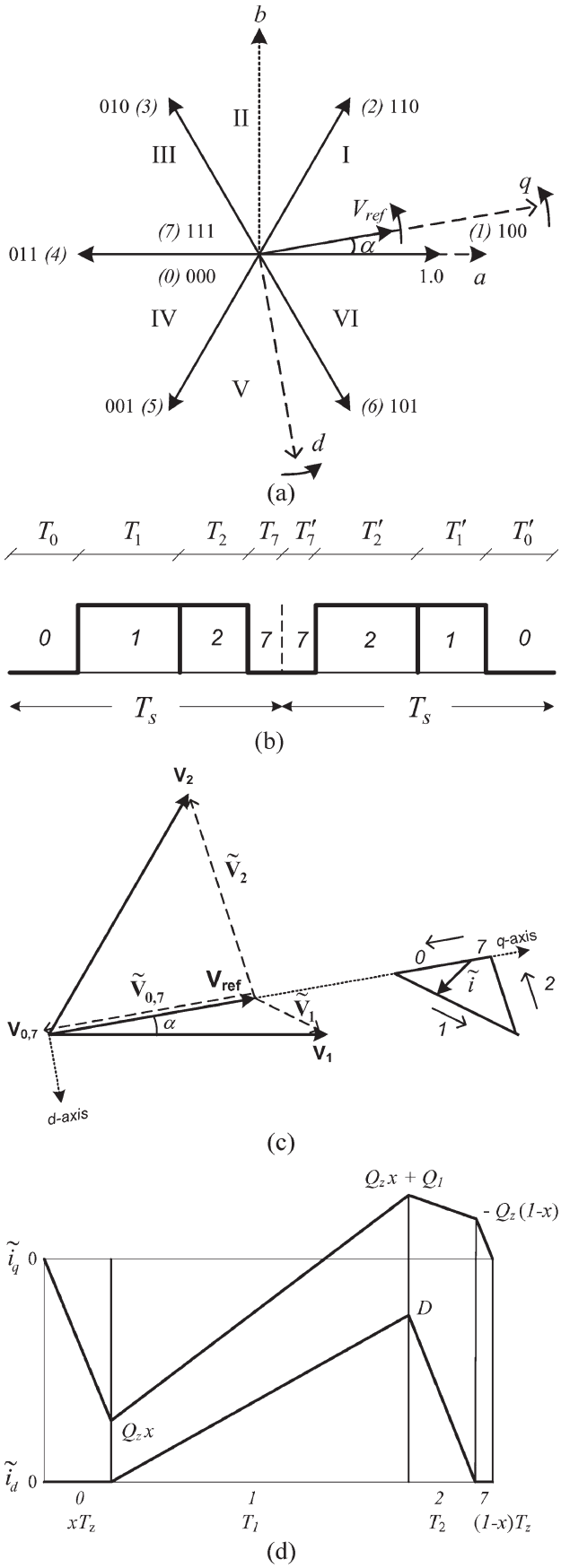

Fig. 1. (a) Voltage vectors of a voltage-source inverter (b) switching sequence (c) trajectory of stator current ripple vector and (d) q-axis and d-axis components of current ripple vector.

The mean square values of the q- and d-axis current ripple over the given subcycle are given in (4a) and (4b), respectively. Equation (4c) gives the total rms current ripple over a subcycle. Thus, we have

$$\begin{aligned}\tilde{i}^2_{q,\mathrm{SUB}} &= \frac{1}{T_s}\int_0^{T_s}\tilde{i}^2_q(t)dt \\ &= \Big[(Q_z x)^2 T_z x + Q_z^2(1-x)^2 T_z(1-x) \\ &\quad + \left\{(Q_z x)^2 + Q_z x(Q_1 + Q_z x)\right. \\ &\quad \left. + (Q_1 + Q_z x)^2\right\} T_1 \\ &\quad + \left\{(Q_1 + Q_z x)^2 + Q_z(1-x) + (Q_1 + Q_z x)\right. \\ &\quad \left. + Q_z^2(1-x)^2\right\} T_2\Big]\left(\frac{1}{3T_s}\right) \end{aligned} \tag{4a}$$

$$\tilde{i}^2_{d,\mathrm{SUB}} = \frac{1}{T_s}\int_0^{T_s}\tilde{i}^2_d(t)dt = \frac{1}{3T_s}\left[D^2(T_1+T_2)\right] \tag{4b}$$

$$\tilde{i}_{\mathrm{SUB}} = \sqrt{\left(\tilde{i}^2_{q,\mathrm{SUB}} + \tilde{i}^2_{d,\mathrm{SUB}}\right)}. \tag{4c}$$

The instantaneous ripple torque produced by the induction motor is proportional to the instantaneous q-axis current ripple, as shown in (5a), where p is the number of poles of the machine, V_{s1} is the peak phase fundamental voltage, ω is the fundamental angular frequency, and σ is the ratio of the total leakage inductance to the magnetizing inductance of the machine [16]. The rms torque ripple over a subcycle is proportional to the corresponding rms q-axis current ripple as shown in the following:

$$\tilde{m}_d = \frac{p}{2}\frac{V_{s1}}{\omega}(1-\sigma)\tilde{i}_q \tag{5a}$$

$$\tilde{m}_{d,\mathrm{SUB}} = \frac{p}{2}\frac{V_{s1}}{\omega}(1-\sigma)\tilde{i}_{q,\mathrm{SUB}}. \tag{5b}$$

III. Optimal Continuous Modulation

The rms current ripple over a subcycle is a function of the fraction x (i.e., T_0/T_z), as shown in (4). While the ratio $x = 0.5$, as in CSVPWM, leads to good spectral properties, this is still suboptimal. The optimal value of x, which results in the minimum rms current ripple over a subcycle for the given reference vector, is given by x_{opt} in

$$x_{\mathrm{opt}} = \frac{(T_z+T_2)}{2T_s} - \frac{Q_1}{Q_z}\frac{(T_1+T_2)}{2T_s}, \qquad 0 \le x_{\mathrm{opt}} \le 1. \tag{6}$$

Substituting for Q_z, Q_1, T_1, T_2, and T_z in (6) using (3) and (1), the optimal duration for which the zero state 0 must be applied, namely, $T_{0(\mathrm{opt})}$, is obtained in terms of V_{ref} and

α, as shown in (7a). The zero state 7 must be applied for the remaining fraction of the duration T_z. That is,

$$T_{0(\text{opt})} = x_{\text{opt}} T_z = 0.5 T_s \left[1 - \frac{7}{3} V_{\text{ref}} \cos(\alpha) + \frac{4}{3} V_{\text{ref}} \cos^3(\alpha)\right] \quad (7a)$$

$$T_{7(\text{opt})} = T_z - T_{0(\text{opt})}. \quad (7b)$$

Expressions have earlier been presented for x_{opt} in terms of three-phase voltage references [6] or three-phase duty ratios [7]. The expression presented in (7) is simpler and does not involve any division during digital implementation.

The rms d-axis current ripple over a subcycle is independent of the fraction x, as seen from (4b). The optimal value of x essentially minimizes the rms q-axis current ripple given in (4a). Consequently, x_{opt} leads to the minimum possible rms torque ripple over the given subcycle for the given reference vector [see (5b)].

IV. Proposed Hybrid PWM

Discontinuous PWM techniques are used in various power electronic applications such as motor drives, front-end converters, and active filters [2], [7], [17]–[19]. These PWM techniques are known to reduce the rms current ripple at higher modulation indexes [2], [6], [7]. With discontinuous modulation, the fraction x is either 1 or 0. If $x = 1$, then the sequence is 012 or 210, where only zero state 0 is used. If $x = 0$, the sequence is 721 or 127, which employs only the zero state 7. There are only two switchings per subcycle with such sequences. Hence, for a given average switching frequency f_{sw}, the subcycle duration can be reduced to two thirds for these sequences, compared to sequence 0127. The reduced subcycle duration could lead to reduced rms torque ripple or rms current ripple, particularly for high values of V_{ref}. Therefore, given a reference vector in sector I, the following three options could be considered in selecting a switching sequence:

1) sequence 0127, with $x = x_{\text{opt}}$ and $T_s = 1/(2f_{\text{sw}})$;
2) sequence 012, with $x = 1$ and $T_s = 1/(3f_{\text{sw}})$;
3) sequence 721, with $x = 0$ and $T_s = 1/(3f_{\text{sw}})$.

The three sequences can be compared in terms of the rms current ripple over a subcycle using (4). The comparison shows that the rms current ripple corresponding to sequence 0127 is the lowest when the tip of the reference vector falls in the spatial region A in Fig. 2(a). Sequences 012 and 721 are the best in terms of the rms current ripple in regions B1 and B2, respectively, in Fig. 2(a). Hence, when the tip of the reference vector falls within region A, sequence 0127 with $x = x_{\text{opt}}$ is employed. When the tip falls in region B1 or B2, sequences 012 or 721, respectively, is used with the subcycle duration reduced to two thirds. Therefore, such a hybrid PWM technique, which is a combination of OCPWM and discontinuous PWM, is termed here as "minimum current ripple PWM" (MCRPWM). This is quite close to the technique presented in [5], which combines CSVPWM and discontinuous PWM.

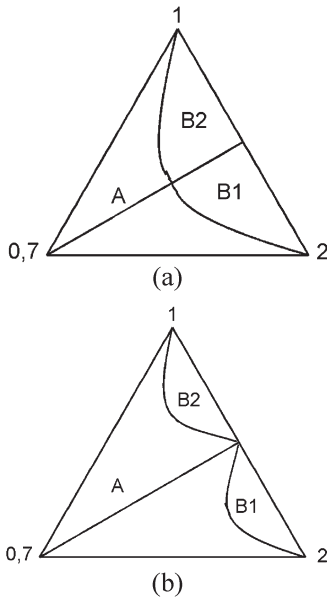

Fig. 2. Hybrid PWM techniques for (a) minimization of rms current ripple (MCRPWM), and (b) minimization of rms torque ripple (MTRPWM) for a given average switching frequency.

A comparison of the three sequences in terms of rms torque ripple or rms q-axis current ripple over a subcycle using (4a) brings out the regions of superior performance of the three, which are shown in Fig. 2(b). Sequence 0127, with the active vectors positioned optimally within the subcycle, leads to the lowest rms torque ripple in region A, as shown in Fig. 2(b). Sequence 012 is better than sequence 721 for $\alpha < 30^\circ$ and vice versa for $\alpha > 30^\circ$. Sequences 012 and 721 are best in regions B1 and B2, respectively, which are symmetric about the center of the sector (i.e., $\alpha = 30^\circ$), as seen in Fig. 2(b).

Hence, the proposed minimum torque ripple PWM (MTRPWM) employs sequences 0127, 7210, ..., with $x = x_{\text{opt}}$ in region A of Fig. 2(b). In region B1, the sequences employed are 012, 210, ..., and in region B2, they are 721, 127, ..., with $T_s = 1/(3f_{\text{sw}})$. Whenever the reference vector falls within region B1 or B2, the rms torque ripple over the given subcycle with MTRPWM is less than that with OCPWM. Hence, MTRPWM results in reduced rms torque ripple over OCPWM at high modulation indexes ($V_{\text{ref}} > 0.73$), as demonstrated in Section V.

CSVPWM, OCPWM, and the hybrid PWM techniques are implemented and tested in an experimental setup consisting of a 5-kVA IGBT-based inverter, a TMS320LF2407 DSP-based digital controller [20], and a four-pole squirrel-cage induction motor characterized by the data given in Table I. The sampling frequency $(1/T_s)$ is 7.2 kHz. The measured no-load current waveforms corresponding to CSVPWM, MCRPWM, and MTRPWM for $V_{\text{ref}} = 0.82$ at a fundamental frequency of 47.3 Hz are shown in Fig. 3.

V. RMS Torque Ripple

In this section, the torque ripple due to the proposed MTRPWM is evaluated and compared against those of CSVPWM

TABLE I
MOTOR PARAMETERS

Output power	3 kW
Speed	1500 RPM
Rated voltage	200 V L-L rms
Frequency	50 Hz
Stator resistance	0.94 Ω
Rotor resistance	0.94 Ω
Stator inductance	183 mH
Rotor inductance	183 mH
Mutual inductance	176 mH

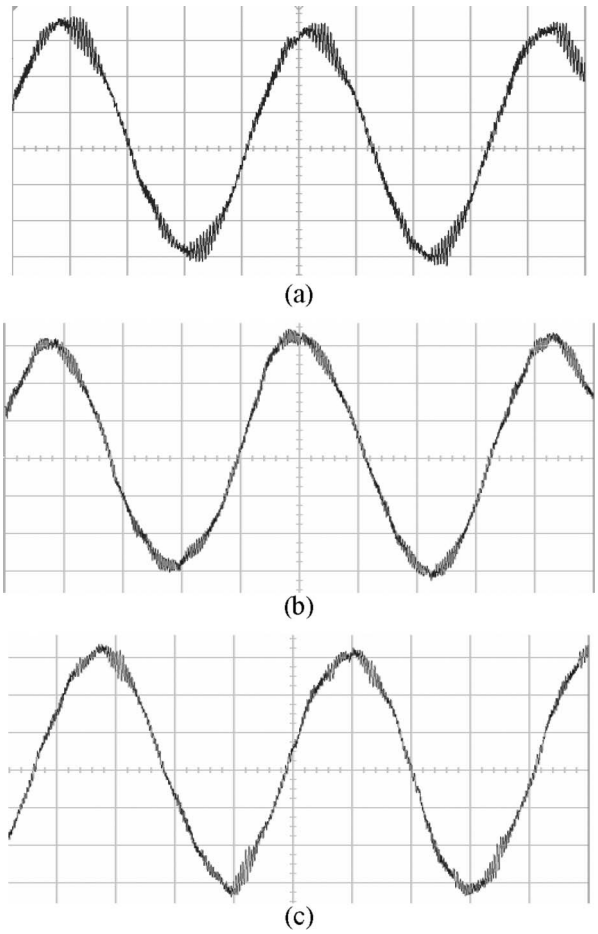

Fig. 3. Experimental line currents corresponding to (a) CSVPWM (b) MCRPWM and (c) MTRPWM for $V_{ref} = 0.82$.

and OCPWM. Theoretical and experimental results are presented.

As discussed in Section II, the pulsating torque is related to the q-axis ripple in the motor currents. The rms q-axis current ripple over a sector or a fundamental cycle can be obtained using the rms q-axis current ripple over a subcycle, as shown in (8a). Correspondingly, the rms torque ripple over a fundamental cycle is derived, as shown in (8b). We have

$$\widetilde{i}_{q,\mathrm{rms}} = \left[\frac{3}{\pi}\int_0^{\frac{\pi}{3}} \widetilde{i}^2_{q,\mathrm{SUB}} d\alpha\right]^{1/2} \tag{8a}$$

$$\widetilde{m}_{d,\mathrm{rms}} = \frac{p}{2}\frac{V_{s1}}{\omega}(1-\sigma)\widetilde{i}_{q,\mathrm{rms}}. \tag{8b}$$

The rms q-axis current ripple, normalized with respect to a base given in (9), is shown plotted against V_{ref} for CSVPWM, OCPWM, and the proposed MTRPWM in Fig. 4(a). The total rms current ripple due to OCPWM has been shown to be only marginally less than that due to CSVPWM ($< 3\%$) [6], [7]. However, the rms q-axis current ripple or the rms torque ripple due to OCPWM is less than that due to CSVPWM by around 19% at $V_{\mathrm{ref}} = 0.86$, as seen in Fig. 4. Thus, the main advantage of OCPWM over CSVPWM is the reduction in rms torque ripple, and not the reduction in current ripple. The proposed MTRPWM results in further reduction in torque ripple for $V_{\mathrm{ref}} > 0.73$. The reduction is around 32% compared to CSVPWM at $V_{\mathrm{ref}} = 0.86$. We have

$$\widetilde{i}_{\mathrm{base}} = \frac{V_{\mathrm{dc}} T_s}{l}. \tag{9}$$

The analytical results have been obtained, considering a simplified harmonic model of the induction motor, namely, its leakage inductance. Simulation results consider a standard induction motor model [4], which is more detailed. Fig. 4(b) shows the rms torque ripple corresponding to the three PWM techniques obtained through simulation for values of V_{ref} ranging from 0.8 to 0.86 in steps of 0.01. These compare well with the corresponding analytical values [solid lines in Fig. 4(b)].

The experimental values of rms torque ripple at steady state are obtained as follows. The measured dc bus voltage and the PWM signals are used to obtain the inverter output voltages. With these terminal voltages and measured motor currents, the instantaneous torque produced by the motor is calculated using a standard motor model [4]. The average torque is subtracted from the instantaneous torque to yield the ripple torque, whose rms value is then calculated.

The experimental values of rms torque ripple for the three techniques are shown in Fig. 4(c). As seen in Fig. 4(b) and (c), there are differences between the simulated and the experimental values of ripple torque. These could be attributed to a number of factors. The device drops and the effect of dead time on the motor terminal voltages are neglected. The dependence of machine parameters (Table I) on frequency is also ignored. Further, the machine model involves assumptions such as negligible depth of slots, sinusoidal magnetomotive force distribution, and magnetic linearity. While these assumptions are valid for the computation of average torque, these could affect the accuracy when used for calculating the ripple torque.

However, the relative values of rms torque ripple due to different PWM techniques obtained through measurement [Fig. 4(c)] tally well with those obtained theoretically

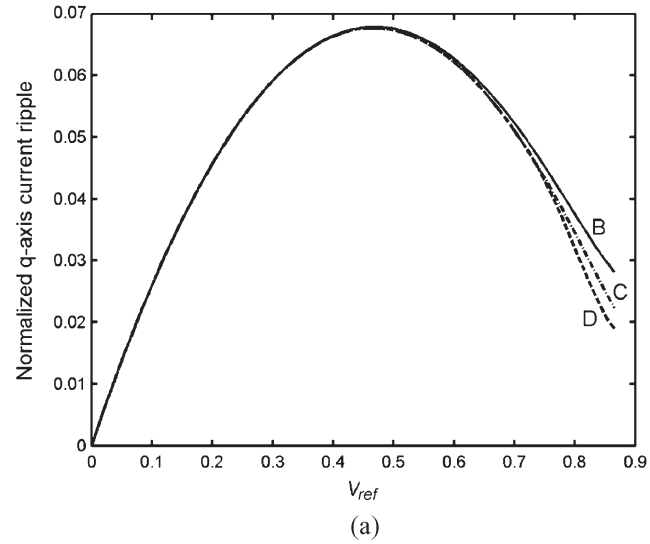

(a)

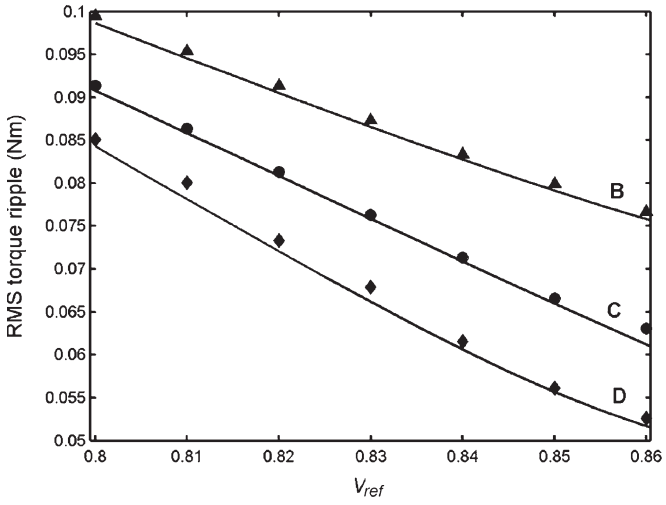

(b)

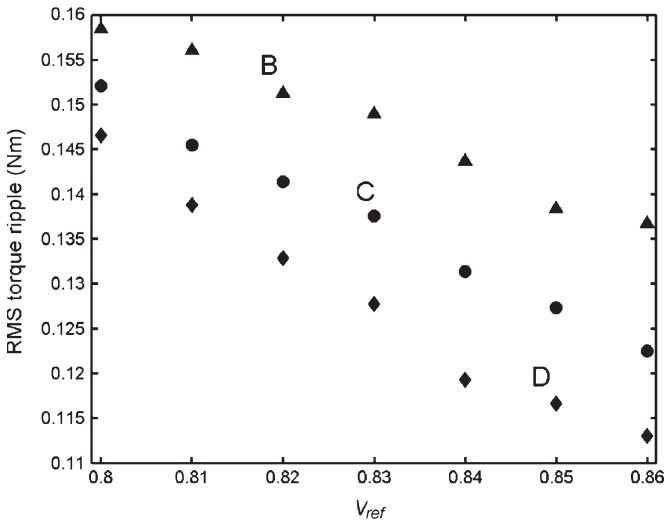

(c)

Fig. 4. Comparison of rms values of torque ripple due to CSVPWM (B), OCPWM (C), and MTRPWM (D). Analytical results (a), simulation results (b), and experimental results (c).

[Fig. 4(b)]. Thus, the proposed MTRPWM is shown to result in less rms torque ripple than both CSVPWM and OCPWM at high modulation indexes.

VI. Conclusion

A hybrid PWM technique has been proposed for the minimization of rms torque ripple in voltage source inverter-fed induction motor drives. The torque ripple due to different PWM techniques are evaluated and compared both theoretically and experimentally. It is shown that OCPWM results in a significant reduction in rms torque ripple over CSVPWM at higher modulation indexes. The proposed MTRPWM, which is a combination of OCPWM and discontinuous PWM, leads to further reduction in rms torque ripple at high speeds of the drive.

References

[1] J. Holtz, "Pulsewidth modulation—A survey," *IEEE Trans. Ind. Electron.*, vol. 39, no. 5, pp. 410–420, Dec. 1992.

[2] D. G. Holmes and T. A. Lipo, *Pulse Width Modulation for Power Converters: Principles and Practice*. Piscataway, NJ: IEEE Press, 2003.

[3] S. Fukuda and Y. Iwaji, "Introduction of the harmonic distortion determining factor and its application to evaluating real time PWM inverters," *IEEE Trans. Ind. Appl.*, vol. 31, no. 1, pp. 149–154, Jan./Feb. 1995.

[4] W. Leonhard, *Control of Electrical Drives*, 3rd ed. New York: Springer-Verlag, 2001.

[5] S. Ogasawara, H. Akagi, and A. Nabae, "A novel PWM scheme of voltage source inverters based on space vector theory," in *Proc. EPE*, Aachen, Germany, Oct. 1989, pp. 1197–1202.

[6] V. Blasko, "Analysis of a hybrid PWM based on modified space-vector and triangle-comparison methods," *IEEE Trans. Ind. Appl.*, vol. 33, no. 3, pp. 756–764, May 1997.

[7] D. Casadei, G. Serra, A. Tani, and L. Zarri, "Theoretical and experimental analysis for the RMS current ripple minimization in induction motor drives controlled by SVM technique," *IEEE Trans. Ind. Electron.*, vol. 51, no. 5, pp. 1056–1065, Oct. 2004.

[8] A. Cataliotti, F. Genduso, A. Raciti, and G. R. Galluzzo, "Generalized PWM–VSI control algorithm based on a universal duty-cycle expression: Theoretical analysis, simulation results, and experimental validations," *IEEE Trans. Ind. Electron.*, vol. 54, no. 3, pp. 1569–1580, Jun. 2007.

[9] M. J. Meco-Gutierez, F. Perez-Hidalgo, F. Vargas-Merino, and J. R. Heredia-Larrubia, "A new PWM technique frequency regulated carrier for induction motors supply," *IEEE Trans. Ind. Electron.*, vol. 53, no. 5, pp. 1750–1754, Oct. 2006.

[10] G. Narayanan and V. T. Ranganathan, "Analytical evaluation of harmonic distortion in PWM AC drives using the notion of stator flux ripple," *IEEE Trans. Power Electron.*, vol. 20, no. 2, pp. 466–474, Mar. 2005.

[11] K. Taniguchi, M. Inoue, Y. Takeda, and S. Morimoto, "A PWM strategy for reducing torque-ripple in inverter-fed induction motor," *IEEE Trans. Ind. Appl.*, vol. 30, no. 1, pp. 71–77, Jan./Feb. 1994.

[12] S. R. Bowes and D. Holliday, "Optimal regular-sampled PWM inverter control techniques," *IEEE Trans. Ind. Electron.*, vol. 54, no. 3, pp. 1547–1559, Jun. 2007.

[13] X. Wu, S. K. Panda, and J. Xu, "Effect of pulse-width modulation schemes on the performance of three-phase voltage source converter," in *Proc. 33rd Annu. IEEE IECON*, 2007, pp. 2026–2031.

[14] G. Narayanan, D. Zhao, H. K. Krishnamurthy, R. Ayyanar, and V. T. Ranganathan, "Space vector based hybrid PWM techniques for reduced current ripple," *IEEE Trans. Ind. Electron.*, vol. 55, no. 4, pp. 1614–1627, Apr. 2008.

[15] K. Zhou and D. Wang, "Relationship between space-vector modulation and three-phase carrier-based PWM: A comprehensive analysis," *IEEE Trans. Ind. Electron.*, vol. 49, no. 1, pp. 186–196, Feb. 2002.

[16] K. Basu, "Minimization of torque ripple in space vector PWM based induction motor drives," M.S. thesis, Indian Inst. Sci., Bangalore, India, 2005.

[17] L. Dalessandro, S. D. Round, U. Drofenik, and J. W. Kolar, "Discontinuous space-vector modulation for three-level PWM rectifiers," *IEEE Trans. Power Electron.*, vol. 23, no. 2, pp. 530–542, Mar. 2008.
[18] L. Asiminoaei, P. Rodriguez, and F. Blaabjerg, "A new generalized discontinuous-PWM strategy for active power filters," in *Proc. 22nd Annu. IEEE APEC*, 2007, pp. 315–321.
[19] L. Asiminoaei, P. Rodriguez, F. Blaabjerg, and M. Malinowski, "Reduction of switching losses in active power filters with a new generalized discontinuous-PWM strategy," *IEEE Trans. Ind. Electron.*, vol. 55, no. 1, pp. 467–471, Jan. 2008.
[20] *TMS320LF/LC240X DSP Controllers Reference Guide (SPRU357)*, Texas Instruments, Dallas, TX, 1990.

Kaushik Basu received the B.Eng. degree from Bengal Engineering and Science University, Shibpore, India, in 2003, and the M.Sc. (Eng.) degree from the Indian Institute of Science, Bangalore, India, in 2005, both in electrical engineering. He is currently working toward the Ph.D. degree in electrical engineering in the Department of Electrical Engineering, University of Minnesota, Minneapolis.

He was with Coldwatt India Private Limited during 2006–2007, where he was responsible for the design and development of high-efficiency power supplies. His major research interests are PWM techniques, motor drives, and magnetics design.

J. S. Siva Prasad received the B.Tech. degree from Nagarjuna University, Andhra Pradesh, India, in 2000, and the M.E. degree from the PSG College of Technology, Coimatore, India, in 2002. He is currently working toward the Ph.D. degree in the Department of Electrical Engineering, Indian Institute of Science, Bangalore, India.

He was with the Department of Energy Systems, Indian Institute of Technology, Bombay, India, from 2002 to 2005, and with Vellore Institute of Technology, Vellore, India, during 2005–2006. His research interests are ac drives, pulsewidth modulation, and design of solar converters.

G. Narayanan (S'99–M'01) received the B.E. degree from Anna University, Chennai, India, in 1992, the M.Tech. degree from the Indian Institute of Technology, Kharagpur, India, in 1994, and the Ph.D. degree from the Indian Institute of Science, Bangalore, India, in 2000.

He is currently an Assistant Professor in the Department of Electrical Engineering, Indian Institute of Science, Bangalore. His research interests include ac drives, pulsewidth modulation, multilevel inverters, and protection of power devices.

Dr. Narayanan received the Innovative Student Project Award for his Ph.D. work from the Indian National Academy of Engineering in 2000 and the Young Scientist Award from the Indian National Science Academy in 2003.